First-principles elastic properties of α-Pu

Per Söderlind and John E. Klepeis
Lawrence Livermore National Laboratory, P.O. Box 808, Livermore, California 94550, USA
(Received 7 November 2008; revised manuscript received 18 February 2009; published 24 March 2009)

Density-functional electronic-structure calculations have been used to investigate the ambient pressure and low temperature elastic properties of the ground-state α phase of plutonium metal. The electronic structure and correlation effects are modeled within a fully relativistic antiferromagnetic treatment with a generalized gradient approximation for the electron exchange and correlation functional. The 13 independent elastic constants, for the monoclinic α-Pu system, are calculated for the observed geometry. A comparison of the results with measured data from recent resonant ultrasound spectroscopy for a cast sample is made.

DOI: 10.1103/PhysRevB.79.104110 PACS number(s): 62.20.de, 71.15.Mb, 71.20.Eh, 71.27.+a

I. INTRODUCTION

Plutonium remains one of the more controversial metals because its complex physics and chemistry are not well understood on a fundamental level. The electronic structure is responsible for many interesting properties of Pu, for instance, an intriguing and unusual phase diagram[1] in which atomic arrangements of sharply contrasting symmetry and density compete closely with each other (see Fig. 1). Although it is generally accepted that this scenario arises from chemical bonding that is flexible enough to accomplish this, the controversy focuses on the description and understanding of the underlying electronic structure. On one hand, dynamical mean-field theory (DMFT) (Ref. 2) may provide a means to describe the electron-correlation effects, while on the other, total energies obtained from density-functional theory (DFT) appear consistent with many ground-state properties of plutonium as well as the aforementioned phase diagram.[3,4]

The only possibility to distinguish these and other models is of course to compare with results of experimental investigations. Fortunately, there have been several recent electronic-structure measurements for Pu (Ref. 5) and a new experiment has been proposed[6] that may help in this regard. Certainly, progress on the theoretical side, DFT, DMFT, or otherwise, provides further motivation for ongoing experimental efforts on plutonium.

Here we are applying DFT to calculate the 13 independent elastic constants of the monoclinic ($P2_1/m$) ground-state α phase of Pu. The result of this investigation is important for several reasons. First, the elastic moduli reflect a detailed picture of the chemical bonding and are therefore relevant when discerning the quality of the electronic structure. Second, single crystal elastic stiffness components for Pu have been measured[7] for δ-Pu, for which theoretical data also exist,[8] but never for the α phase. The present results therefore serve as predictions and could be used for comparison with other models or to constrain semiempirical descriptions[9,10] of α-Pu.

In Sec. II we review technical details of the computational method including our theoretical model for α-Pu. This is followed by Sec. III in which we report calculated elastic constants and relate these to data on cast α-Pu. We discuss some sensitivities of the elastic properties with respect to the atomic volume, structural relaxations, inclusion of spin polarization, spin-orbit (SO) coupling, and orbital polarization (OP) in Sec. IV. Finally, we provide some concluding remarks in Sec. V and a detailed description of the strains applied to the lattice and the corresponding elastic constants in the Appendix.

II. COMPUTATIONAL DETAILS

The electronic structure and total energy for α-Pu are obtained from density-functional calculations which require the crystal geometry and the atomic number (94 for Pu). The monoclinic crystal structure has been determined by x-ray diffraction[11] and is rather complex with 16 atoms/cell. It is characterized by eight atomic positions, two axial ratios, and a unique non-90-degree angle. Theoretically it is in principle possible to allow all parameters of this structure to relax, but the associated computational burden makes it prohibitive with the present technique. However, our previous study of the α-Pu structure[12] leads us to believe that relaxation effects are rather small. We will discuss this further in Sec. IV.

For the experimental geometry[11] very small strains ($\leq 1\%$) are applied so that the elastic constants can be extracted using relevant equations which are, for completeness, included in the Appendix. About four to eight magnitudes of strains are used for every elastic constant and a fourth degree

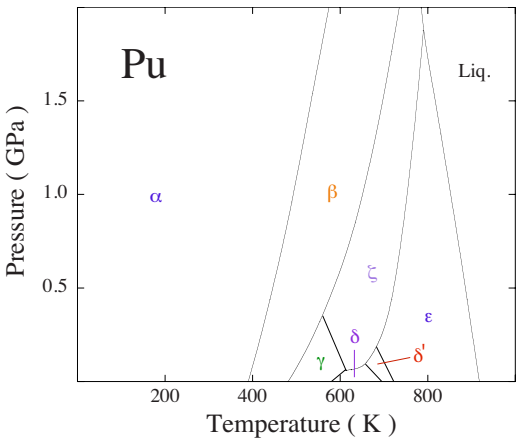

FIG. 1. (Color online) The experimental (Ref. 1) phase diagram of Pu.

TABLE I. Present calculations without orbital polarization and published with orbital polarization (Ref. 3) (SO+OP) together with those neglecting spin polarization and SO (no SO). Atomic volumes, V, in Å^3 and bulk moduli, B, in GPa. Experimental data (Refs. 17 and 18) are for cast α-Pu. B_{fix} is the bulk modulus evaluated at 20.3 Å^3.

Method	V	B	B_{fix}
Present theory	19.0	59	25
SO+OP	20.3	50	50
No SO	17.3	218	81
Expt.	20.2–20.4	46.6–54.4	

polynomial is fitted to the corresponding energies thus defining the harmonic coefficient, relevant for the elastic constants [Eq. (A2)]. In all cases, fitting to a second-order polynomial gives a result not different by more than about 10%. The use of higher orders of polynomials does not change the results significantly. No structural relaxation is allowed during the strain because of computational limitations. This approximation, however, was shown to be justified for the elastic-constant calculation of α-U (Ref. 13) and we believe this is the case also for α-Pu. Nonetheless, it is plausible that allowing such relaxations could lower the elastic energies a small amount.

Electron correlations are more pronounced in Pu than most other metals. Here, these effects are modeled by the generalized gradient approximation,[14] spin polarization, and SO coupling. This approach is the same as has been used for Pu in the past[3,12] with the exception of the OP present in the previous scheme. Although ideally preferred, inclusion of OP severely impacts the efficiency of the computations and for the demanding task of calculating the elastic constants for α-Pu this complication is neglected. The effect of OP is known to be substantial for δ-Pu (Refs. 15 and 16) but electron-correlation effects are weaker in α-Pu. In Table I we contrast data obtained from calculations for α-Pu with and without OP, together with recent measurements for cast α-Pu. We notice that OP expands the equilibrium volume, resulting in a very close agreement with room-temperature data.[17,18] The theoretical bulk moduli compare favorably with the measurement as well. All elastic constants are computed using a fixed volume for the unstrained lattice [V_0; Eq. (A1)] and because the OP equilibrium volume is in better agreement with experiment we chose this value (V_0 =20.3 Å^3).

For the present calculations we use a full-potential version of the linear muffin-tin orbital method implemented by Wills *et al.*[19] The use of full nonsphericity of the charge density and one-electron potential is essential for accurate total energies and in particular when elastic constants are calculated. This is accomplished by expanding the charge density and potential in cubic harmonics inside nonoverlapping muffin-tin spheres and in a Fourier series in the interstitial region. In all calculations we use two energy tails associated with each basis orbital and for 6s, 6p, and the valence states (7s, 7p, 6d, and 5f) these pairs are different. With this "double basis" approach we include six energy tail parameters and 12 basis

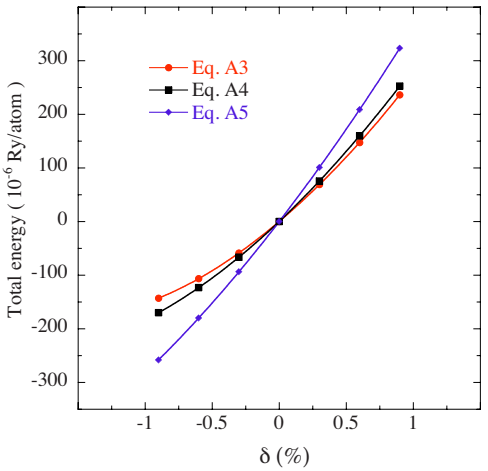

FIG. 2. (Color online) Total energy (μRy/atom) as a function of strain parameter (δ). The symbols denoted Eqs. A3–A5 correspond to the strains defined by Eqs. (A3)–(A5) in the Appendix.

functions per atom. Spherical harmonic expansions are carried out through l_{max}=6 for the basis, potential, and charge density. The sampling of the irreducible Brillouin zone (BZ) is done using the special k-point method[20] and 54 k points are utilized for this purpose. Test calculations increasing this number to 128 result in no significant change in the elastic constants (less than 3%). To each energy eigenvalue a Gaussian is associated with 20 mRy width to speed up convergence. Spin-orbit coupling is implemented in a first-order variational procedure[21] for the valence d and f states, as was done previously,[3] and for the core states the fully relativistic Dirac equation is solved. Total energies are converged to the μRy/atom level which typically requires about 100 self-consistent-field cycles.

III. ELASTIC CONSTANTS

Only in the last few years calculations of elastic constants for more complex geometries have been attempted from first

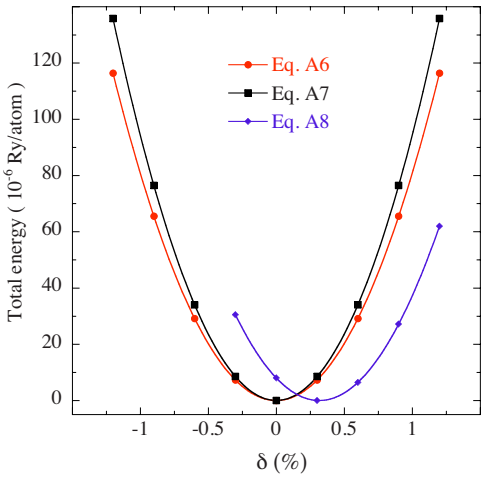

FIG. 3. (Color online) Total energy (μRy/atom) as a function of strain parameter (δ). The symbols denoted Eqs. A6–A8, correspond to the strains defined by Eqs. (A6)–(A8) in the Appendix.

TABLE II. Elastic coefficients (GPa) associated with the strains defined by Eqs. (A3)–(A15) in the Appendix.

A3	A4	A5	A6	A7	A8	A9	A10	A11	A12	A13	A14	A15
120.0	108.8	86.2	43.4	50.6	43.7	247.4	204.0	217.9	301.8	255.0	87.6	126.4

principles, such as our own study on PtSi which is an eight atom/cell orthorhombic system.[22] More recently the elastic constants of coesite, a monoclinic high-pressure polymorph of silica, were calculated[23] and these compared favorably with experimental data. Another low-symmetry system, α-U (a closer neighbor to Pu), has been investigated within DFT and the obtained elastic properties agree well between various computations[13,24,25] and measured data.

Here, we present the first calculated elastic constants for α-Pu, a material with a high degree of complexity both with regard to the crystal and electronic structures. The monoclinic lattice has 13 independent moduli which can be determined from the total-energy response to small distortions. A general elastic constant, c_{ij}, is obtained at a fixed unstrained atomic volume (V_0) through Eq. (A1) given in the Appendix. The 13 applied strains, all summarized in the Appendix, depend on a distortion parameter δ.

In Fig. 2 we show the total energies as functions of δ for the strains defined in Eqs. (A3)–(A5) which relate to c_{11}, c_{22}, and c_{33}, respectively. These elastic constants are associated with elongations along the x, y, and z directions. Because these strains are not conserving the atomic volume (the determinants of the corresponding strain matrices are not unity) the total energy is only lowest for the unstrained lattice if the calculation is performed at the theoretical equilibrium volume. Here the total energies are computed at a volume of 20.3 Å^3, which is somewhat larger than the calculated equilibrium volume (19.0 Å^3) (see Table I), as discussed in Sec. II. This then immediately explains why a negative δ, which compresses the lattice, lowers the total energy in Fig. 2. Notice also in this figure that these axial strains [Eqs. (A3)–(A5)] show parallel dependence on δ. The similarity of these curves suggests that the volume dependence of b/a and c/a is small.

In Fig. 3 we show the total energies for the strains defined by Eqs. (A6)–(A8). These strains correspond to the elastic constants c_{44}, c_{55}, and c_{66}, which are associated with the angle between the respective axes. One of these lowers the total energy a minute amount for a 0.25% strain, suggesting that the experimental structure is not the lowest-energy structure in the calculations but very close. Overall, however, the total-energy dependencies on these strains, combined with the remaining ones [Eqs. (A9)–(A15), not shown], suggest that the theoretical treatment reproduces the details of the monoclinic structure remarkably well.

In Table II we present the calculated elastic coefficient (C) associated with each strain, defined in the Appendix. The first six strains [Eqs. (A3)–(A8)] immediately define the elastic constants c_{ii}, whereas the other strains [Eqs. (A9)–(A15)] give linear combinations of c_{ij}. The number of independent equations equals the number of unknown elastic moduli resulting in a well-defined system of linear equations that can be solved straightforwardly. Notice in Table II that all distortions give rise to elastic coefficients that are relatively large and positive (smallest is 43 GPa), implying mechanical stability with respect to all 13 strains.

Next, by solving the linear equations for the c_{ij}, we collect the entries in Table III. Some of the elastic constants, such as c_{12} for example, are negative but this should not be interpreted as an instability because the actual applied distortions all give rise to positive elastic coefficients, as mentioned above. It is also evident that $c_{11} \approx c_{22}$ while c_{33} is smaller. This likely means that the c/a axial ratio is more sensitive to external influences, such as pressure and temperature, than the b/a axial ratio.

The bulk modulus (B) is a special elastic constant that is related to a uniform change in the atomic density or volume. On one hand, it can be directly obtained from calculations of the total energy as a function of the atomic volume (equation of state). In practice, the total energy is often fitted to an analytical expression which defines B. In our case we use the Murnaghan form[26] for this purpose, and the results are presented in Table I. On the other hand, B can be evaluated from the elastic compliance constants s_{ij} (tabularized in Table IV), which are components of the inverse to the elastic-constant matrix,[23]

$$B^{-1} = s_{11} + s_{22} + s_{33} + 2(s_{12} + s_{13} + s_{23}). \quad (1)$$

Computing B from the equation of state yields a value of 25 GPa (Table I), whereas using Eq. (1) (after first numerically inverting the elastic-constant matrix) gives 21 GPa. The fact that the bulk modulus obtained from these independent approaches agrees reasonably well indicates a consistency of the calculations but also reveals some numerical uncertainties because they are not identical.

As mentioned in Sec. I, there are no experimental single crystal elastic constants to compare with our theoretical counterparts. Instead we attempt to relate our results to polycrystal data. Recently Migliori *et al.*[17] determined quantities they labeled as c_{11} and c_{44} from their resonant ultrasound

TABLE III. Elastic constants (GPa) obtained from the calculated elastic coefficients given in Table II combined with Eqs. (A3)–(A15) in the Appendix.

c_{11}	c_{22}	c_{33}	c_{44}	c_{55}	c_{66}	c_{12}	c_{13}	c_{23}	c_{15}	c_{25}	c_{35}	c_{46}
120.0	108.8	86.2	43.4	50.6	43.7	−9.30	1.10	−11.5	2.21	2.02	2.19	−0.25

TABLE IV. Elastic compliance constants (10^{-3} GPa^{-1}) obtained from inverting the elastic-constant matrix (Table III).

s_{11}	s_{22}	s_{33}	s_{44}	s_{55}	s_{66}	s_{12}	s_{13}	s_{23}	s_{15}	s_{25}	s_{35}	s_{46}
9.52	10.9	14.0	23.0	28.3	22.9	2.03	1.58	3.10	−5.65	−6.58	−8.00	0.13

spectroscopy measurements of longitudinal and shear sound speeds of arc-cast α-Pu. The latter refers to an isotropic shear modulus, G, while the former we will call $\tilde{c}_{11}$ to distinguish it from the single crystal c_{11}. For an isotropic material they are related to the bulk modulus through the equation

$$B = \tilde{c}_{11} - \frac{4G}{3}. \tag{2}$$

Thus, we can collate the measured[17,18] B, $\tilde{c}_{11}$, and G with our calculated single crystal elastic constants using Eqs. (1) and (2) and an estimated value for the shear modulus,

$$G_V = \frac{1}{15}[c_{11} + c_{22} + c_{33} + 3(c_{44} + c_{55} + c_{66}) - (c_{12} + c_{13} + c_{23})]. \tag{3}$$

This is the Voigt upper bound[27] on the effective shear modulus for a macroscopically isotropic polycrystal and it gives us B=21, G=G_V=49.9, and $\tilde{c}_{11}$=87.5 GPa, compared to[17,18] 46.6–54.4, 43.5–43.7, and 104.6–112.8 GPa. Since we are using the Voigt upper bound for the shear modulus, but the exact expression [Eq. (1)] for the bulk modulus, it is interesting to also use the Voigt upper bound for the bulk modulus to be consistent with the shear modulus,

$$B_V = \frac{1}{9}[c_{11} + c_{22} + c_{33} + 2(c_{12} + c_{13} + c_{23})]. \tag{4}$$

This then gives us slightly different values which are summarized and compared with experimental data in Table V. Clearly in Table V, the theoretical bulk modulus agrees least favorably with that of experimental data, while both G and $\tilde{c}_{11}$ are closer. In addition, G_V is larger than the observed value which is expected because it represents an upper bound. It should be mentioned that DFT elastic constants are often within 10%–20% of measurements which is the case here for both G and $\tilde{c}_{11}$.

IV. DISCUSSION

Although attempts to model the electronic structure as accurate as possible are made, we do neglect the effect of orbital polarization to make the calculations computationally feasible. To partly compensate for this, we choose to evaluate the elastic constants at the equilibrium volume obtained from the more complete electronic-structure treatment that includes OP. In addition, we do not perform structural relaxations but assume the experimental crystal structure.

Next, we explore the uncertainties associated with these simplifications. A complete structural relaxation is not possible with the techniques applied here but relaxations of the axial ratios and the monoclinic angle are. We do this by optimizing each parameter separately, guided by the total energy, starting from the observed structure.[11] For α-Pu this is easy because our calculations reproduce the experimental data very accurately (b/a=1.77, c/a=0.75, and θ=102°). The atomic positions were relaxed in a previous study using another technique[12] and agreed well with the measured data.[11] Consequently, for the unstrained lattice, it is appropriate to assume insignificant issues with relaxation and to use the experimental geometry close to the equilibrium volume (~20 Å^3). But, as already mentioned, no relaxation is allowed during the very small (≤1%) elastic-constant distortions.

Now we investigate the influence of orbital polarization by collating calculations for the c_{11} elastic constant. In Fig. 4 we show the total-energy variation as a function of strain associated with c_{11} for models including both spin-orbit coupling and orbital polarization (SO+OP) and spin-orbit coupling only (SO). The atomic volume for the unstrained lattice

TABLE V. Presently calculated Voigt averages of B, G, and $\tilde{c}_{11}$ together with experimental data (Refs. 17 and 18) for cast α-Pu. The unit is GPa.

Method	B	G	$\tilde{c}_{11}$
Present theory	30.6	49.9	97.1
Expt.	46.6–54.4	43.5–43.7	104.6–112.8

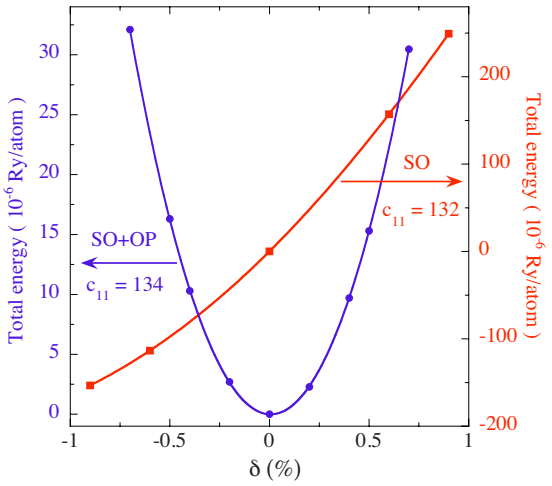

FIG. 4. (Color online) Total energy (μRy/atom) as a function of strain parameter (δ) corresponding to the c_{11} elastic constant [Eq. (A3)]. The unstrained atomic volume is 20.3 Å^3. The blue solid-circle symbols (left y axis) denote results obtained from a model including both spin-orbit coupling and orbital polarization (SO+OP). The red solid-square symbols (right y axis) refer to a model with spin-orbit coupling only (SO). The solid lines are the polynomial fits used to extract c_{11} (see main text). The shown c_{11} is given in units of GPa.

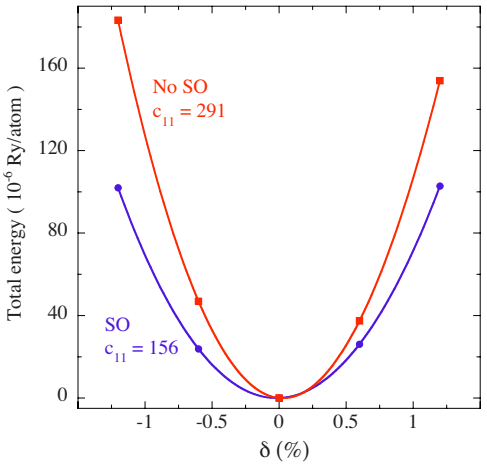

FIG. 5. (Color online) Total energy (μRy/atom) as a function of strain parameter (δ) corresponding to the c_{11} elastic constant [Eq. (A3)]. The blue solid-circle symbols denote results obtained from a model including spin-orbit coupling (SO). The red solid-square symbols refer to a model with neither spin polarization nor spin-orbit coupling (no SO). The solid lines are the polynomial fits used to extract c_{11} (see main text). The calculations are performed for the respective equilibrium volumes (Table I). The shown c_{11} is given in units of GPa.

is chosen to be that of the equilibrium for the (SO+OP) treatment (V_0=20.3 Å^3). First we observe that for the SO +OP approximation the total energy is minimized for the unstrained crystal (δ=0). This result suggests that axial ratios and the atomic volume are relaxed. This is not the case for the model with spin-orbit interaction only (SO) for which negative δ lowers the atomic volume closer to the calculated equilibrium (19.0 Å^3) with a lowering of the total energy as a result. Nevertheless, the computed c_{11} are nearly identical for the two approaches with a difference of about 1.5%. These results (132 and 134 GPa) are somewhat larger than the tabulated value (120 GPa; see Table III) because the calculations shown in Fig. 4 are only for comparison between the models and are modified as follows: first, we employ 16 k points in the irreducible BZ (not 54) and second, the Fourier series expansion used to represent the electron potential and density in the interstitial is decreased by about 15%. These technical changes decrease the computational burden about 1 order of magnitude which in turn allows us to introduce and test the influence of orbital polarization.

Thus, from Fig. 4 it appears that our approach of neglecting OP but performing the calculations at the equilibrium volume of the full treatment is a good compromise. When evaluated at 19.0 Å^3 (not shown) all elastic coefficients are larger by about 20%–45%. As a consequence, $\tilde{c}_{11}$ and G [Eq. (2)] are both about 35% larger at this smaller V_0 and in disagreement with the experimental data (see Table V). The increase in the elastic coefficients is mostly due to greater attractive 5f bonding and also because the moduli scale inversely with V_0 [Eq. (A1)].

Because it is likely that orbital polarization has a minor influence on the α-Pu elastic constants the question arises if spin-orbit interactions and spin polarization could likewise be neglected as a reasonable approximation. In Fig. 5 we again show total-energy results associated with the c_{11} elastic constant, now for a model with spin-orbit interaction and spin polarization (SO) and one without (no SO). First we notice that the unstrained lattice (δ=0) gives the minimum energy for both models. This is a consequence of properly relaxed axial ratios and unstrained (V_0) atomic volume. It is evident that these two models predict significantly different c_{11}. Both spin-orbit coupling and spin polarization reduce the effective occupation of bonding 5f-electron states thus weakening the overall bond strength. The result is a lower density, bulk modulus, and elastic constants. Ignoring these electron-correlation effects leads to an overestimation of the aforementioned properties and the results shown in Fig. 5 suggest that it is rather severe for α-Pu. When evaluated at the SO +OP equilibrium volume (20.3 Å^3) there is an improvement, particularly for the simplest (no SO) model (SO+OP: 134, SO: 132, and no SO: 139 GPa). Nonetheless, the (no SO) treatment is worsening c_{11} and better calculations (SO) are feasible and preferred.

V. CONCLUSION

We have reported the theoretical elastic constants for α-Pu. The electron-correlation effects are modeled by an antiferromagnetic spin configuration[3] including spin-orbit coupling. The elastic-constant calculations in conjunction with unit-cell relaxations imply that the experimentally observed monoclinic structure[11] is stable and very close to what is predicted by the theory. Also, the b/a and c/a axial ratios are shown to be rather similar in their dependence on external influences such as pressure or temperature, with the c/a likely being more sensitive.

The strains applied to α-Pu [Eqs. (A3)–(A15)] result in elastic coefficients ranging from 43 to 302 GPa. This is in stark contrast to the elastic behavior of δ-Pu for which the tetragonal shear constant is much smaller[7] ($c' \sim 5$ GPa). One interpretation of this distinct elastic behavior is that the 5f-electron bonding provides a mechanically less stable situation in δ-Pu relative to α-Pu and that δ-Pu is closer to a structural phase transition (a lower phase transformation barrier).

Test calculations of the c_{11} elastic constant suggest that orbital polarization may not be necessary when spin-orbit interaction is included and the volume is chosen to be that of the OP calculation which is also close to the experimental volume ($\sim$20.3 Å^3). The computed elastic properties serve as predictions and can be used as benchmark for other theories or for development of interatomic potentials and semiempirical models for α-Pu. Although an indirect comparison, present calculated single crystal elastic constants do not appear to be inconsistent with reported data from polycrystal α-Pu (see Table V). The largest relative difference with experiment is for the bulk modulus which is small when evaluated at 20.3 Å^3 but better when obtained at the equilibrium volume (Table I). The bulk modulus is very soft in α-Pu and small absolute differences between calculations can be large in relative terms. Inclusion of orbital polarization certainly improves the calculations for the bulk modulus while it may not necessarily influence the elastic constants significantly.

Another plausible reason for the discrepancy between calculations and measurements is the uncertainty of comparing single crystal calculations with polycrystal data. The single crystal elastic moduli must be averaged to enable a comparison and the inherent uncertainty with this procedure is difficult to estimate. Future experiments on single crystal α-Pu could resolve this issue.

Last, our calculations do not address thermal lattice vibrations whereas the measurements are performed at room temperature. The elastic constants show very pronounced softening with temperature[17] and it was proposed that this behavior is linked to $5f$-electron localization. Our own investigations[28,29] (not shown) of α-Pu, employing Debye-Grüneisen methodology and other quasiharmonic treatments, suggest that the thermal softening of the moduli can largely be accounted for by quasiharmonic phonon contributions with no temperature dependence of the electronic structure. If this is true, $5f$-electron localization is probably not the primary driver for the thermal softening of the moduli.

ACKNOWLEDGMENTS

J. Pask is acknowledged for help with matrix manipulations. R. Rudd is thanked for helpful discussions. This work was performed under the auspices of the U.S. Department of Energy by Lawrence Livermore National Laboratory under Contract No. DE-AC52-07NA27344.

APPENDIX

In this appendix, we present the strains of the monoclinic (α-Pu) structure applied to calculate the 13 independent elastic constants of this phase. The internal energy of a crystal under strain, δ, can be Taylor expanded in powers of the strain tensor with respect to that of the unstrained crystal in the following way:

$$E(V,\delta) = E(V_0,0) + V_0\left(\sum_i \tau_i \xi_i \delta_i + \frac{1}{2}\sum_{i,j} c_{ij}\delta_i\xi_i\delta_j\xi_j\right) + O(\delta^3). \tag{A1}$$

The volume of the unstrained system is denoted V_0 and $E(V_0,0)$ is this system's internal energy, which corresponds to the total energy obtained from the electronic structure. The Voigt notation has been used in the equation above, i.e., xx, yy, zz, yz, xz, and xy are replaced with 1–6. Of course, yz, xz, and xy are equal to zy, zx, and yx and for that reason ξ_i is equal to 1 for $i=1,2,3$ and 2 for $i=4,5,6$. τ_i above is a component of the stress tensor. In practice this equation is here used for all 13 strains and the equation can be written as

$$E(V,\delta) = E(V_0,0) + V_0\left(\tau\delta + \frac{1}{2}C\delta^2\right), \tag{A2}$$

where we have introduced τ representing a linear combination of stress components and C, a linear combination of elastic constants. C will be specified below as we introduce the various strains, while we are not concerned here about the stress terms. Next, we present the strains and their corresponding elastic coefficients C,

$$\begin{pmatrix} 1+\delta & 0 & 0 \\ 0 & 1 & 0 \\ 0 & 0 & 1 \end{pmatrix}, \quad C = c_{11}, \tag{A3}$$

$$\begin{pmatrix} 1 & 0 & 0 \\ 0 & 1+\delta & 0 \\ 0 & 0 & 1 \end{pmatrix}, \quad C = c_{22}, \tag{A4}$$

$$\begin{pmatrix} 1 & 0 & 0 \\ 0 & 1 & 0 \\ 0 & 0 & 1+\delta \end{pmatrix}, \quad C = c_{33}, \tag{A5}$$

$$\frac{1}{(1-\delta^2)}\begin{pmatrix} 1 & 0 & 0 \\ 0 & 1 & \delta \\ 0 & \delta & 1 \end{pmatrix}, \quad C = 4c_{44}, \tag{A6}$$

$$\frac{1}{(1-\delta^2)}\begin{pmatrix} 1 & 0 & \delta \\ 0 & 1 & 0 \\ \delta & 0 & 1 \end{pmatrix}, \quad C = 4c_{55}, \tag{A7}$$

$$\frac{1}{(1-\delta^2)}\begin{pmatrix} 1 & \delta & 0 \\ \delta & 1 & 0 \\ 0 & 0 & 1 \end{pmatrix}, \quad C = 4c_{66}, \tag{A8}$$

$$\frac{1}{(1-\delta^2)}\begin{pmatrix} 1+\delta & 0 & 0 \\ 0 & 1-\delta & 0 \\ 0 & 0 & 1 \end{pmatrix}, \quad C = c_{11} + c_{22} - 2c_{12}, \tag{A9}$$

$$\frac{1}{(1-\delta^2)}\begin{pmatrix} 1+\delta & 0 & 0 \\ 0 & 1 & 0 \\ 0 & 0 & 1-\delta \end{pmatrix}, \quad C = c_{11} + c_{33} - 2c_{13}, \tag{A10}$$

$$\frac{1}{(1-\delta^2)}\begin{pmatrix} 1 & 0 & 0 \\ 0 & 1+\delta & 0 \\ 0 & 0 & 1-\delta \end{pmatrix}, \quad C = c_{22} + c_{33} - 2c_{23}, \tag{A11}$$

$$\frac{1}{(1-\delta^2)}\begin{pmatrix} 1+\delta & 0 & \delta \\ 0 & 1-\delta & 0 \\ 0 & 0 & 1 \end{pmatrix}, \quad C = c_{11} + c_{22} + c_{55} - 2(c_{12} - c_{15} + c_{25}), \tag{A12}$$

$$\frac{1}{(1-\delta^2)}\begin{pmatrix} 1+\delta & 0 & \delta \\ 0 & 1 & 0 \\ 0 & 0 & 1-\delta \end{pmatrix}, \quad C = c_{11} + c_{33} + c_{55} - 2(c_{13} - c_{15} + c_{35}), \tag{A13}$$

$$\begin{pmatrix} 1 & \delta & 0 \\ 0 & 1 & \delta \\ 0 & 0 & 1 \end{pmatrix}, \quad C = c_{44} + c_{66} + 2c_{46}, \tag{A14}$$

$$\frac{1}{(1+\delta)} \begin{pmatrix} 1+\delta & 0 & \delta \\ 0 & 1 & 0 \\ 0 & 0 & 1 \end{pmatrix}, \quad C = c_{11} + c_{55} + 2c_{15}. \tag{A15}$$

[1] D. A. Young, *Phase Diagrams of the Elements* (University of California Press, Berkeley, 1991).

[2] A. Georges, G. Kotliar, W. Krauth, and W. Rozenberg, Rev. Mod. Phys. **68**, 13 (1996); A. B. Shick and V. A. Gubanov, Europhys. Lett. **69**, 588 (2005); L. V. Pourovskii, M. I. Katsnelson, A. I. Lichtenstein, L. Havela, T. Gouder, F. Wastin, A. B. Shick, V. Drchal, and G. H. Lander, *ibid.* **74**, 479 (2006).

[3] P. Söderlind, Europhys. Lett. **55**, 525 (2001); P. Söderlind and B. Sadigh, Phys. Rev. Lett. **92**, 185702 (2004).

[4] G. Robert, A. Pasturel, and B. Siberchiot, J. Phys.: Condens. Matter **15**, 8377 (2003); Europhys. Lett. **71**, 412 (2005).

[5] G. van der Laan, K. T. Moore, J. G. Tobin, B. W. Chung, M. A. Wall, and A. J. Schwartz, Phys. Rev. Lett. **93**, 097401 (2004); J. G. Tobin, K. T. Moore, B. W. Chung, M. A. Wall, A. J. Schwartz, G. van der Laan, and A. L. Kutepov, Phys. Rev. B **72**, 085109 (2005); K. T. Moore, G. van der Laan, R. G. Haire, M. A. Wall, and A. J. Schwartz, *ibid.* **73**, 033109 (2006); K. T. Moore, G. van der Laan, M. A. Wall, A. J. Schwartz, and R. G. Haire, *ibid.* **76**, 073105 (2007); K. T. Moore, G. van der Laan, R. G. Haire, M. A. Wall, A. J. Schwartz, and P. Söderlind, Phys. Rev. Lett. **98**, 236402 (2007); J. G. Tobin, P. Söderlind, A. Landa, K. T. Moore, A. J. Schwartz, B. W. Chung, M. A. Wall, J. M. Wills, R. G. Haire, and A. L. Kutepov, J. Phys.: Condens. Matter **20**, 125204 (2008); K. T. Moore and G. van der Laan, Rev. Mod. Phys. **81**, 235 (2009).

[6] S. W. Yu, J. G. Tobin, and P. Söderlind, J. Phys.: Condens. Matter **20**, 422202 (2008).

[7] J. Wong, M. Krisch, D. L. Farber, F. Occelli, A. J. Schwartz, Tai-C. Chiang, M. Wall, C. Boro, and R. Xu, Science **301**, 1078 (2003).

[8] O. Eriksson, J. D. Becker, A. V. Balatsky, and J. M. Wills, J. Alloys Compd. **287**, 1 (1999); X. Dai, S. Y. Savrasov, G. Kotliar, A. Migliori, H. Ledbetter, and E. Abrahams, Science **300**, 953 (2003); P. Söderlind, A. Landa, B. Sadigh, L. Vitos, and A. Ruban, Phys. Rev. B **70**, 144103 (2004).

[9] M. I. Baskes, Phys. Rev. B **62**, 15532 (2000).

[10] J. A. Moriarty, J. F. Belak, R. E. Rudd, P. Söderlind, F. H. Streitz, and L. H. Yang, J. Phys.: Condens. Matter **14**, 2825 (2002).

[11] W. H. Zachariasen, Acta Crystallogr. **5**, 660 (1952); **5**, 664 (1952).

[12] B. Sadigh, P. Söderlind, and W. G. Wolfer, Phys. Rev. B **68**, 241101(R) (2003).

[13] P. Söderlind, Phys. Rev. B **66**, 085113 (2002).

[14] J. P. Perdew, J. A. Chevary, S. H. Vosko, K. A. Jackson, M. R. Pederson, D. J. Singh, and C. Fiolhais, Phys. Rev. B **46**, 6671 (1992).

[15] P. Söderlind, Phys. Rev. B **77**, 085101 (2008).

[16] F. Cricchio, F. Bultmark, and L. Nordström, Phys. Rev. B **78**, 100404(R) (2008).

[17] A. Migliori, I. Mihut, J. B. Betts, M. Ramos, C. Mielke, C. Pantea, and D. Miller, J. Alloys Compd. **444-445**, 133 (2007).

[18] O. J. Wick, *Plutonium Handbook A Guide to the Technology* (Gordon and Breach, New York, 1967).

[19] J. M. Wills, O. Eriksson, M. Alouani, and D. L. Price, in *Electronic Structure and Physical Properties of Solids*, edited by H. Dreysse (Springer-Verlag, Berlin, 1998), p. 148.

[20] D. J. Chadi and M. L. Cohen, Phys. Rev. B **8**, 5747 (1973); S. Froyen, *ibid.* **39**, 3168 (1989).

[21] O. K. Andersen, Phys. Rev. B **12**, 3060 (1975).

[22] O. Beckstein, J. E. Klepeis, G. L. W. Hart, and O. Pankratov, Phys. Rev. B **63**, 134112 (2001).

[23] H. Kimizuka, S. Ogata, and J. Li, J. Appl. Phys. **103**, 053506 (2008).

[24] C. D. Taylor, Phys. Rev. B **77**, 094119 (2008).

[25] J. Bouchet, Phys. Rev. B **77**, 024113 (2008).

[26] F. D. Murnaghan, Proc. Natl. Acad. Sci. U.S.A. **30**, 244 (1944).

[27] J. P. Watt, J. Appl. Phys. **51**, 1520 (1980).

[28] P. Söderlind (unpublished).

[29] L. Benedict (unpublished).